Highlights of Spanish Astrophysics XII, Proceedings of the XVI Scientific Meeting of the Spanish Astronomical Society held on July 15 - 19, 2024, in Granada, Spain. M. Manteiga, F. González Galindo, A. Labiano Ortega, M. Martínez González, N. Rea, M. Romero Gómez, A. Ulla Miguel, G. Yepes, C. Rodríguez López, A. Gómez García and C. Dafonte (eds.), 2025

Towards an astronomical use of new generation geodetic observations - Imaging and astronomical results

Pérez-Díez, V.[1,3], Martí-Vidal, I.[2,4], and Albentosa-Ruiz, E.[2]

[1] Observatorio Astronómico Nacional (OAN-IGN), Alfonso XII 3, 28014 Madrid, Spain
[2] Dpt. Astronomia i Astrofísica, Universitat de València, C/ Dr. Moliner 50, 46120 Burjassot, Spain
[3] Centro de Desarrollos Tecnológicos, Observatorio de Yebes (IGN), 19141 Yebes, Guadalajara, Spain
[4] Observatori Astronòmic, Universitat de València, C/ Cat. José Beltrán 2, 46980 Paterna, Spain

Abstract

We introduce a new imaging method for wide bandwidth very-long-baseline-interferometry (VLBI) data, specifically from the VLBI Global Observing System (VGOS). By including genetic algorithms in traditional Regularized-Maximum-Likelihood (RML) imaging methods, we optimize imaging results for our study cases, enabling multi-frequency images to extract extensive information from celestial sources. Starting from the calibrated data with a new pipeline based on the PolConvert software, we can obtain full-polarization images, unlocking valuable insights into Active-Galactic-Nuclei (AGN) characteristics like shape, jet morphology, magnetic fields, core shift, and Faraday rotation. VGOS's ability to observe numerous sources simultaneously facilitates comprehensive multi-source studies, promising transformative advancements in AGN research and improving geodetic observables by including the polarized structure of the sources.

1 Introduction

The VLBI Global Observing System (VGOS) (10) is the next-generation geodetic VLBI system coordinated by the International VLBI Service for Geodesy and Astrometry (IVS) [1]. It uses ultra-wideband linear-polarized receivers (2 to 14 GHz) to achieve high-precision geodetic measurements (7).

To calibrate VGOS data, the most commonly used calibration method involves the pseudo-Stokes I (pI) approach (2), which handles total intensity but cannot extract information about the polarized brightness distribution of the observed sources. To address this challenge, the European project EU-VGOS (1) decided to use PolConvert (8), a software tool that allows the transformation of linear-polarized data into a circular-polarization basis. This conversion allows the use of legacy VLBI

[1]https://ivscc.gsfc.nasa.gov/index.html

Table 1: Sources most commonly observed in experiment VO2187.

Source	N_{obs}	N_{scan}
1849+670	1004	60
2229+695	987	61
1803+784	836	66
0059+581	692	59
0613+570	625	46
3C418	532	56
0955+476	392	52
3C274	203	39
DA426	177	43
OJ287	168	37

calibration algorithms designed for circular-polarization receivers, enabling the retrieval of full Stokes parameters (I, Q, U, and V) from the data.

Another aspect that negatively affects geodetic observables is the impact of source structure and astrometric image alignment among the four VGOS frequencies. Hence, obtaining full-polarization and wide-band images from VGOS observations would contribute to both improve the geodetic data and provide valuable astronomical information from the sources. By imaging each band separately using closure quantities (4), absolute spatial information is lost, so it is not possible to astrometrically align the four bands. For this reason, multi-frequency regularized maximum likelihood (RML) imaging has been used in this work, which allows us to obtain better images of the sources and achieve consistent inter-band astrometry.

2 Observations and data calibration

We tested our method on the IVS experiment with code VO2187, observed on 6-7 July 2022. The eight participating antennas were Goddard (GS), Ishioka (IS), Kokee (K2), McDonald (MG), the twin Onsala telescopes (OE and OW), Westford (WF), and Yebes (YJ).

The full recorded bandwidth was 1 GHz, divided into 32 spectral windows (spw) of 32 MHz each, across a wide frequency coverage between 3 GHz and 11 GHz. The bands, centered around 3.25, 5.5, 6.75, and 10.5 GHz, respectively, are labeled following the convention of the VGOS community: A, B, C, and D.

A total of 74 sources (radio-loud AGN) were observed during about 24 hours, in short interleaved scans with a typical duration of 30 s. In Table 1, we list the sources on which more observing time was spent, and for which full-polarization images were generated. Sources are ordered by the number of observations (N_{obs}, which is the sum of the number of baselines per scan, over all scans and N_{scan} is the number of scans).

The data calibration procedure can be found in (11) and is summarized in the following lines:

We used the software `PolConvert` (8) that computes and applies the X/Y bandpass (accounting for the phase-cal tones) to convert from linear to circular polarization. Then, we apply a Wideband

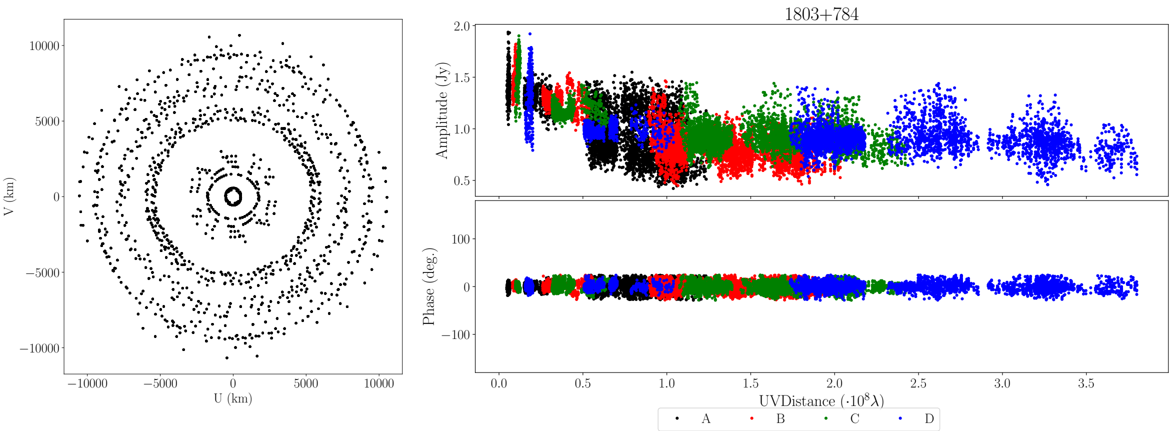

Figure 1: Visibility plots for source 1803+784. **Left**, UV coordinates. **Right**, amplitudes (top) and phases (bottom) of the RR and LL visibilities as a function of distance in Fourier space (in units of wavelength). The different VGOS bands are shown in different colors.

Global Fringe Fitting (WBGFF) algorithm, implemented in the `PyPhases` module of `PolConvert`, that removes the bulk of the dispersive Ionosphere effects using IONEX models of Total Electron Content (TEC), performs an ordinary Global Fringe Fitting (to estimate an effective delay across the full band) and solves for the residual dispersive component by fitting a new model of the antenna gains. An example of calibrated data for one source can be seen in Fig. 1.

3 Imaging

We employed RML algorithms for imaging, based on the use of closure information. This approach streamlines the calibration process, as station-based calibration errors are mitigated by using these observables. Additionally, this method enables super-resolution, which is beneficial for studying source-structure effects.

Specifically, we used the `EHTim` software (3), which has recently incorporated a multifrequency mode for image deconvolution (5). This method applies a two-term log-log Taylor expansion around a reference image I_0 at a reference frequency ν_0:

$$\log I_i = \log(I_0) + \alpha \log\left(\frac{\nu_i}{\nu_0}\right) + \beta \log^2\left(\frac{\nu_i}{\nu_0}\right) + \dots, \tag{1}$$

where α corresponds to the spectral index map and β represents the spectral curvature map.

This approach is particularly advantageous for VGOS data, as it incorporates information from four separate frequency bands to produce a combined intensity-versus-frequency map. A further benefit is the ability to align images across different bands, allowing the study of structural properties such as core shifts.

We have developed a genetic algorithm method to optimize the selection of the deconvolution parameters. To evaluate the performance, we first generate synthetic datasets that mimic realistic observational scenarios. The simulation includes various types of sources, like point sources, fake jet-like sources and real images. These synthetic datasets allow us to evaluate the robustness of deconvolution algorithms across a range of astrophysical source types.

The simulated source models are then used to generate synthetic observations, where the effects of limited uv-coverage, bandwidth, and noise are incorporated. This step simulates the data acquisition process of the VGOS array. We perform image deconvolution using various combinations of regularizers and their weights, field-of-view sizes, data weights, number of iterations and different ways of self-calibration.

To assess the quality of each deconvolved image, we compute the structural similarity index (SSIM) between the deconvolved image and the original input model used to generate the synthetic observations. Specifically, we use the DSSIM metric (the dissimilarity version of SSIM), which provides a perceptual measure of the visual difference between two images by approximating human vision. The goal is to minimize DSSIM, thus achieving a deconvolved image that closely resembles the original.

We use a genetic algorithm to optimize the imaging parameters. It's implemented using the PyGAD library, an open-source Python tool for creating genetic algorithms and optimizing machine learning models. Our genetic algorithm operates by evolving a population of candidate parameter sets through selection, crossover, and mutation, with the fitness function being the DSSIM score. Parallelization techniques are employed to speed-up the optimization process, with the deconvolution of different parameter sets distributed across multiple CPU cores. This ensures that the large search space of regularizers, weights, fields of view, and iterations is efficiently explored.

Through this process, we obtain the set of deconvolution parameters that yields the best reconstruction quality for our specific observational configuration, source types, and data characteristics. Then, we apply these parameters to the image deconvolution of the real VGOS data.

Fig. 2 presents total intensity maps for each VGOS band, all convolved to the same beam to facilitate comparison. By displaying images from different frequencies side by side, we can analyze the core shift. The features observed in these images, including the jet's direction and extent, are consistent with surveys conducted by other arrays at comparable frequencies.

In Fig. 3, we present full-polarization images of the source 1849+670, produced using the `CASA` version of CLEAN, across the four VGOS bands. These images were obtained following a D-term calibration performed with the software `PolSolve` (9).

The total-intensity distributions in Fig. 3 (black contours) reveal a jet extending northwest, consistent with the jet orientation published by the MOJAVE program (6). The positions of the polarization intensity peaks (yellow crosses) are also aligned with the jet direction relative to the total-intensity peaks, although a slight counterclockwise rotation is observed from bands A to C. Notably, the polarization peak in band D coincides with the total-intensity peak at the resolution of CLEAN. Interestingly, the anticipated core shift would suggest that the total-intensity core should shift southeast at higher frequencies (opposite to the jet direction). However, we observe the polarization peak moving closer to the total-intensity peak at higher frequencies. If the polarization peak were associated with an optically thin jet feature, we would expect the opposite behavior, with the distance between the polarization and total-intensity peaks increasing with frequency. The fact that the polarization peak behaves as observed implies that the polarized emission originates from an optically thick region.

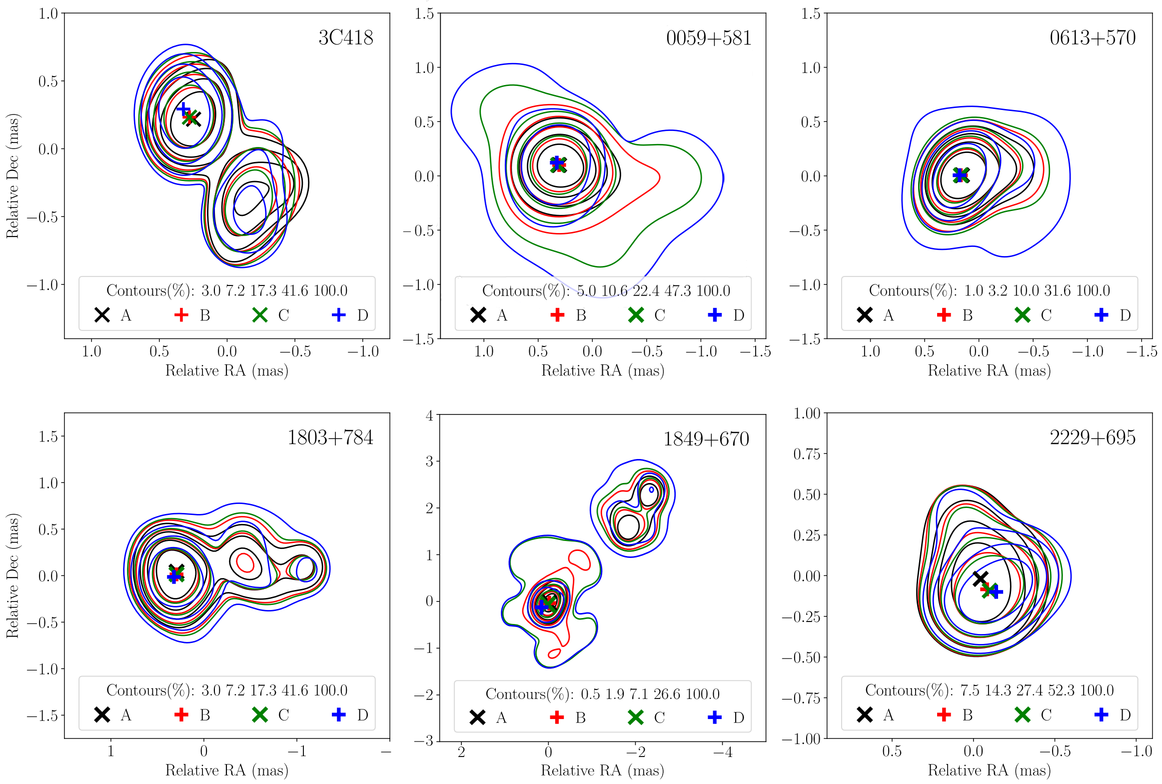

Figure 2: Total intensity maps from VGOS experiment VO2187. The contours are shown at five levels of the peak percentage, specified in the legend of the plots. Each contour color represents the map for the central frequency of each band: 3.25, 5.5, 6.75, and 10.5 GHz.

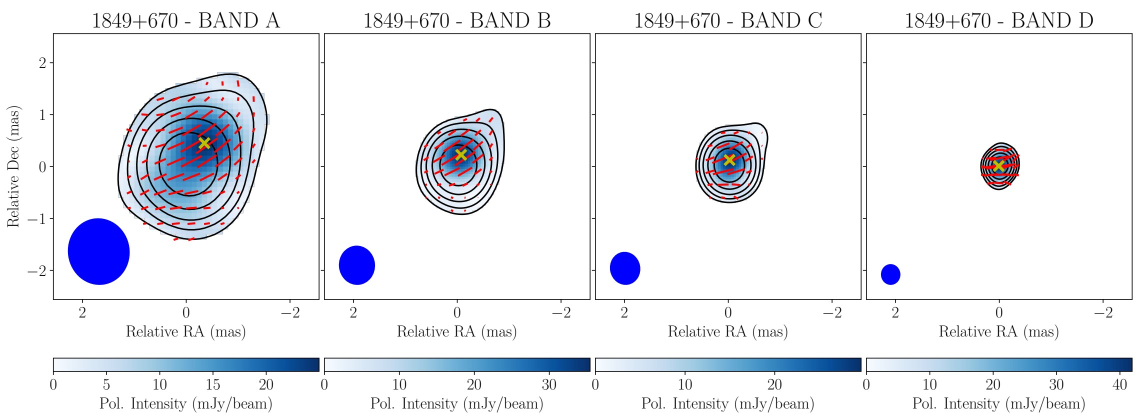

Figure 3: CLEAN full-polarization images of 1849+670 for epoch VO2187, using all the VGOS bands. The FWHM of the convolving beams are shown in the bottom left corners. Contours are shown at five levels of peak percentage in logarithmic scale. The polarization intensity is shown in blue, EVPAs are shown in red, and the polarization peaks are marked as yellow crosses.

The EVPA (electric vector position angle) values at the polarization intensity peaks are 56.3, 56.7, 67.5, and 81.2 degrees for bands A through D, respectively. These results do not follow the expected λ^2 law for Faraday-thin external rotation-measure screens, further indicating that the region emitting the polarized radiation is optically thick.

4 Conclusions

We have developed a complete calibration process for VGOS observations that can be also used in other wideband VLBI data. This process allows us to study the instrumental and source-intrinsic polarization and to obtain information on all Stokes parameters.

Using RML multi-frequency imaging, we obtain very reliable maps of the sources. To achieve greater reliability of the images, we have developed a genetic algorithm that optimizes the selection of parameters for deconvolution. These images can be used to study the effects of source structure in geodetic products. This, together with obtaining full-polarization images, allows us to study AGN properties, such us the core-shift, spectral indices, jet morphology and its variation over time.

Acknowledgments

This work has been partially supported by the Generalitat Valenciana Projects CIDEGENT/2018/021 and ASFAE/2022/018, as well as the MICINN Research Projects PID2019-108995GB-C22 and PID2022-140888NB-C22. We acknowledge support from the Astrophysics and High Energy Physics programme by MCIN, with funding from European Union NextGenerationEU (PRTR-C17I1).

References

[1] Alef, W., Anderson, J. M., Bernhart, S., et al. 2019, in Proceedings of the 24th European VLBI Group for Geodesy and Astrometry Working Meeting, Vol. 24, 107–111

[2] Cappallo, R. 2014, in International VLBI Service for Geodesy and Astrometry 2014 General Meeting Proceedings, 91–96

[3] Chael, A., Johnson, M. D., Narayan, R., et al. 2016, ApJ, 829, 11

[4] Chael, A., Johnson, M. D., Bouman, K. L., et al. 2018, ApJ, 857, sd

[5] Chael, A., Issaoun, S., Pesce, D. W., et al. 2023, ApJ, 945, 40

[6] Lister, M. L., Aller, M. F., Aller, H. D., et al. 2018, ApJS, 234, 12

[7] Niell, A., Barrett, J., Burns, A., et al. 2018, Radio Science, 53, 1269

[8] Martí-Vidal, I., Roy, A., Conway, J., & Zensus, A. J. 2016, A&A, 587, A143

[9] Martí-Vidal, I., Mus, A., Janssen, M., de Vicente, P., & González, J. 2021, A&A, 646, A52

[10] Petrachenko, B., Niell, A., Behrend, D., et al. 2009, Design Aspects of the VLBI2010 System. Progress Report of the IVS VLBI2010 Committee, June 2009., NASA/TM-2009-214180, 2009, 62 pages

[11] Pérez-Díez, V, Martí-Vidal, I., Albentosa-Ruiz, E. 2024, A&A, 688 (2024) A151